Proceedings of the ASME 2015 International Design Engineering Technical Conferences & Computers and Information in Engineering Conference
IDETC/CIE 2015
August 2-5, 2015, Boston, Massachusetts, USA

DETC2015-47852

A THEORETICAL INVESTIGATION OF THE CRITICAL TIMESCALES NEEDED FOR DIGGING IN DRY SOIL USING A BIOMIMETIC BURROWING ROBOT

Monica Isava
Dept. of Mechanical Engineering
Massachusetts Institute of Technology
Cambridge, Massachusetts 02139
Email: misava@mit.edu

Amos G. Winter, V
Dept. of Mechanical Engineering
Massachusetts Institute of Technology
Cambridge, Massachusetts 02139
Email: awinter@mit.edu

ABSTRACT

RoboClam is a bio-inspired robot that digs into underwater soil efficiently by expanding and contracting its valves to fluidize the substrate around it, thus reducing drag. This technology has potential applications in fields such as anchoring, sensor placement, and cable installation. Though there are similar potential applications in dry soil, the lack of water to advect the soil particles prevents fluidization from occurring. However, theoretically, if the RoboClam contracts quickly enough, it will achieve a zero-stress state that will allow it to dig into dry soil with very little drag, independent of depth. This paper presents a theoretical model of the two modes of soil collapse to determine how quickly a device would need to contract to achieve this zero-stress state. It was found that a contraction time of 0.02 seconds would suffice for most soils, which is an achievable timescale for a RoboClam-like device.

INTRODUCTION

RoboClam is a bioinspired robot that imitates the up/in/down/out valve motion pattern of the Atlantic razor clam, *Ensis directus*, in order to burrow into underwater soil using an order of magnitude less energy than would be required to push a blunt body to the same depth [1]. Potential applications for this technology exist in fields such as anchoring, oil recovery, cable installation, and sensor placement.

RoboClam digs via localized fluidization: as it contracts its valves, the soil and water around it mix in the remaining void, creating a substance that behaves as a viscous Newtonian fluid. In the region of localized fluidization, the substrate provides much less resistance to penetration compared to static soil. After the robot pushes down, it reopens its valves to repeat the process again [1].

The minimum and maximum contraction and expansion times required to achieve fluidization have been reported in prior work [1]. Minimum contraction time is determined by Stokes drag [2], or the amount of time it takes the fluid to advect a soil particle and reach the valve velocity during contraction. This timescale is dependent on the density and diameter of soil particles, as well as the density of the fluid. For 1mm diameter glass beads (which can represent a typical sand) submerged in water, this analysis yields a minimum contraction time of 0.075s [1].

Maximum contraction time is determined by the time it would take the soil to naturally collapse and landslide around the mechanism, which can be determined by determining the forces acting on a collapsing element of soil. This timescale depends on the distance the soil must slide (the contraction distance), the densities of the particles and fluid, the void fraction of the soil (the fraction of volume that is taken up by fluid rather than by particles), and the failure angle of the soil (the angle at which it will naturally landslide). Again, using 1mm glass beads submerged in water, and using the contraction distance of the current RoboClam (0.00285m), we get a maximum contraction time of 0.20s [1].

Lastly, the maximum expansion time is determined by the amount of time it takes the soil to settle. Settling time is determined by the height of the contracting mechanism and the void fraction of the soil [3]. For 1mm glass beads and the current dimensions of RoboClam, this analysis yields a maximum expansion time of 2.2s [1].

Beyond the submerged soil applications mentioned above, there are also potential dry soil applications for RoboClam-like burrowing. Sensor placement, in particular, is desirable in dry conditions as well as in underwater environments. However, fluidization theory does not apply to dry soil for two reasons: first, the interstitial air exerts much less drag on the soil particles than water, making it unable to advect the particles into the void around the contracting device. Second, the change in void fraction makeup will make the settling time for dry soil much faster than for submerged soil, so the theoretical

maximum expansion time is void as well. Therefore, in order to have a RoboClam-like device dig into dry soil, a new theoretical approach must be developed. This paper describes such a theoretical approach that shows that RoboClam's motions can be used to dig into dry soil within a range of time scales that may be achievable by a machine.

STRESS STATE ANALYSIS

In order to determine whether a RoboClam-like mechanism will be able to dig through dry soil, we analyze the stress state of the soil around the end effector before and after contraction. Figure 1 shows a Mohr's circle analysis of the initial stress state of the soil. There is an initial vertical effective stress, σ_{v0}', and an initial horizontal effective stress, σ_{h0}', which together define the Mohr's circle, or the complete stress state. Effective stress refers to the actual stress between particles, neglecting any pore pressure. Additionally, Figure 1 shows the incipient failure stress state of the soil, which is defined as the point at which slow contraction would result in soil failure. Soil failure is achieved when the Mohr's circle of the soil hits the soil's failure envelope (which is determined by φ, the friction angle of that particular soil), because at this point the shear force in the soil has exceeded the shear strength of the soil [4]. As the mechanism contracts, the horizontal stress decreases but the vertical stress stays the same (as the vertical stress is defined by the mass of the soil above it, which does not change) [4]. The decreasing horizontal stress causes the Mohr's circle to enlarge until it becomes tangent to the failure envelope, at which point the soil starts to fail. If a device were to contract slowly, the soil around it would fail when the horizontal stress reached σ_{hf}'.

Figure 2 shows an analysis of a rapidly contracting device. If a mechanism were to contract quickly enough to bring the horizontal stress state close to zero, then the corresponding Mohr's circle would have a vertical stress state close to zero as well. It is impossible for a soil to exist in a stress state where the Mohr's circle goes beyond the failure envelope, so the resulting Mohr's circle must be tangent to the failure envelope. This imbalance of vertical and horizontal stresses resembles the stress state of the soil at ground level, where RoboClam can dig easily. If a device is able to contract quickly enough to achieve this zero-stress state, then it will be able to easily penetrate dry soil no matter how deep it is. From an engineering perspective, it is important to determine how quickly the contraction must occur in order to achieve a zero-stress state. In order to answer this question, the different mechanisms of soil failure must be investigated.

TYPES OF SOIL COLLAPSE

There are two ways that soil can fail around a contracting RoboClam-like device, both of which can be derived by looking at soil failure using a cylindrical coordinate system. Figure 3 shows both failure scenarios: a radial-vertical stress imbalance and a radial-hoop stress imbalance [5].

A radial-vertical stress imbalance occurs when, after contraction of the device, the radial stress decreases while the vertical stress remains constant, to the point where the radial-vertical Mohr's circle is tangent to the failure envelope. This failure mode can be likened to a "landslide" collapse around the device, where soil slides diagonally into the void left by the contracting mechanism (Fig 4).

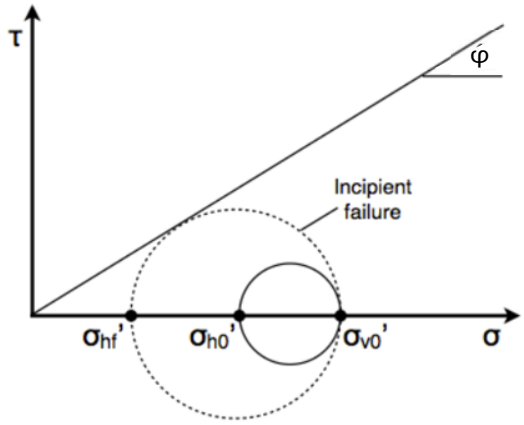

Figure 1: INITIAL STRESS STATE OF SOIL (DENOTED WITH A SOLID LINE), AND INCIPIENT FAILURE STRESS STATE, DENOTED BY THE DOTTED LINE. The incipient failure state is found by decreasing the horizontal stress until the failure state is tangent to the stress envelope, and corresponds to the moment at which the soil starts to collapse around a mechanism that has just contracted. Labels: τ is shear stress, σ is normal stress, φ is the friction angle of the soil; subscripts h and v are horizontal and vertical, respectively; subscript 0 indicates initial state; subscript f indicates failure state; and superscript prime indicates effective stress, which are the actual stresses between soil particles (neglecting hydrostatic pressure)

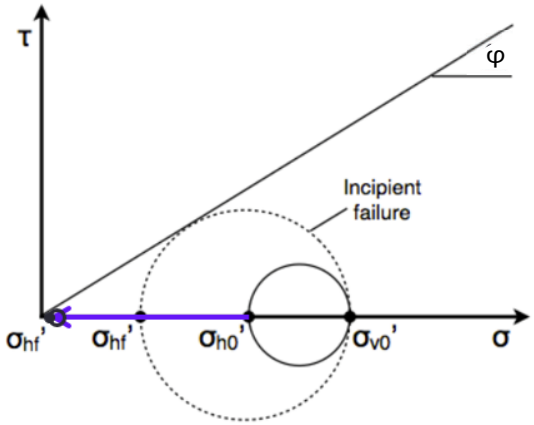

Figure 2: ZERO-STRESS STATE INDUCED BY REDUCING HORIZONTAL STRESS BELOW INCIPIENT FAILURE. As the horizontal stress decreases along the purple arrow, the failure circle shrinks until both the vertical and horizontal stresses are near zero, mimicking the stress state the soil experiences at the surface. Initial stress state and incipient failure circle are included for reference.

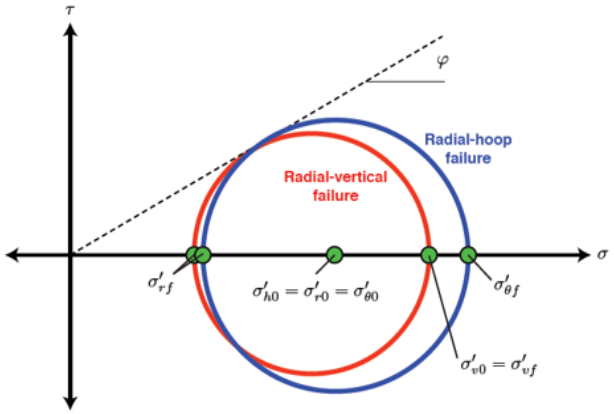

Figure 3: FAILURE SCENARIOS IN SOIL COLLAPSING AROUND ROBOCLAM. The red circle corresponds to a scenario in which the vertical stress remains constant while the radial stress decreases until the Mohr's circle is tangent to the failure envelope. This is a radial-vertical stress imbalance. The blue circle corresponds to a scenario in which the radial and hoop stresses start off equal (as the original horizontal stress) and the radial stress decreases while the hoop stress increases until the Mohr's circle is tangent to the failure envelope. This is a radial-hoop stress imbalance.

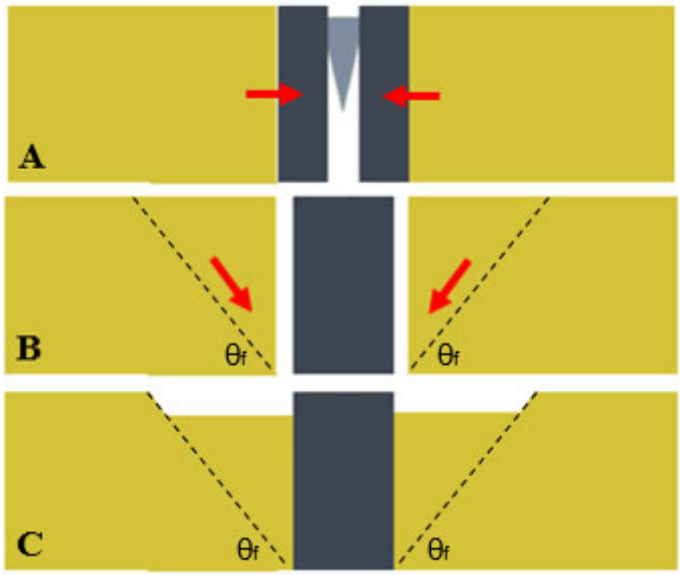

Figure 4: PROGRESSION OF RADIAL-VERTICAL FAILURE, OR "LANDSLIDE" COLLAPSE, SIDE VIEW. The end effector contracts as denoted by the red arrows in step A, leaving a void around it in step B. Between steps B and C, the soil falls along the failure angle θ_f as denoted by the red arrows in step B. In step C, the soil around the void has fallen diagonally to fill the void.

A radial-hoop stress imbalance occurs when the radial and hoop stresses (which both are equal to the horizontal stress before contraction) diverge to the point where the radial-hoop Mohr's circle is tangent to the failure envelope; that is, the radial stress, which decreases as the device contracts, and the hoop stress, which increases as the device contracts, together define a Mohr's circle that is tangent to the failure envelope. This failure mode can be likened to "annular" collapse around the device, where, when looked at from above, a "ring" of soil collapses simultaneously to fill the void left by the contracting device (Fig 5).

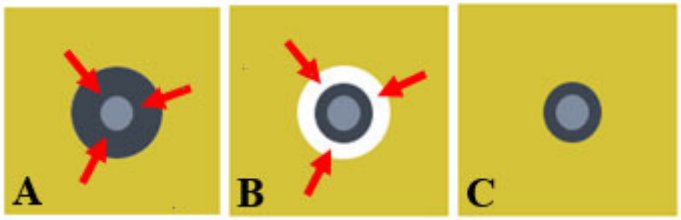

Figure 5: PROGRESSION OF RADIAL-HOOP FAILURE, OR "ANNULAR" COLLAPSE, TOP VIEW. The end effector contracts as shown by the red arrows in step A, leaving a void around it in step B. In between steps B and C, the soil around the void collapses radially, as denoted by the red arrows in step B. In step C, the ring of soil around the void has collapsed and filled the void.

COLLAPSING SOIL MODELED AS A THICK-WALLED PRESSURE VESSEL

In order to quantify the physics of the soil collapse, we propose a thick-walled pressure vessel model. To simplify the analysis, a few assumptions are made: first, we assume the mechanism is infinitely long in order to neglect end effects. Second, we assume that the depth of the mechanism is much greater than its length (h>>L) in order to consider stresses along the length of the device to be uniform. Lastly, we assume that the device contraction is quasi-static and that the soil can be modeled as an elastic solid since it is not being sheared and plastically deforming before contraction. These three assumptions allow us to model the collapsing soil around the contracting device, at the moment just before failure, as a thick-walled pressure vessel [6].

The thick-walled pressure vessel model will only hold for a linear elastic solid, which is only true of the soil before it begins to shear due to failure. Therefore, we model the soil as a pressure vessel for the moment just after contraction, but before failure. This analysis will allow us to determine the amount of soil that will fail around the contracting device. Figure 6 shows a diagram of the thick-walled pressure vessel model. The mechanism is shown in dark gray as having just contracted, with a failure zone denoted in green around it. The pressure vessel is the substrate around the failure zone, spanning from the outer edge of the failure zone to the edge of soil failure an unknown distance away. Since the mechanism has just contracted, the outer edge of the pressure vessel has not yet felt the effects of the change in pressure on the inner edge of the vessel. Thus, the stress state of the soil on the outer edge of the vessel can be likened to the stress state of soil at an undisturbed point an infinite horizontal distance away. Starting with the

original thick-walled pressure vessel equations [7], and modifying them to reflect geotechnical convention (with compressive stresses positive) and an outer radius that approaches infinity (to represent the undisturbed soil at the outer edge of the pressure vessel, some unknown distance away), we get

$$\sigma_r = \frac{R_0^2(p_i - p_0)}{r^2} + p_0 \tag{1}$$

$$\sigma_\theta = \frac{-R_0^2(p_i - p_0)}{r^2} + p_0 \tag{2}$$

where σ_r is the radial stress, σ_θ is the hoop stress, R_0 is the radius of the expanded mechanism, p_i is the pressure in the void, p_0 is the lateral pressure of the undisturbed soil at infinity, or the initial horizontal pressure of the soil before contraction.

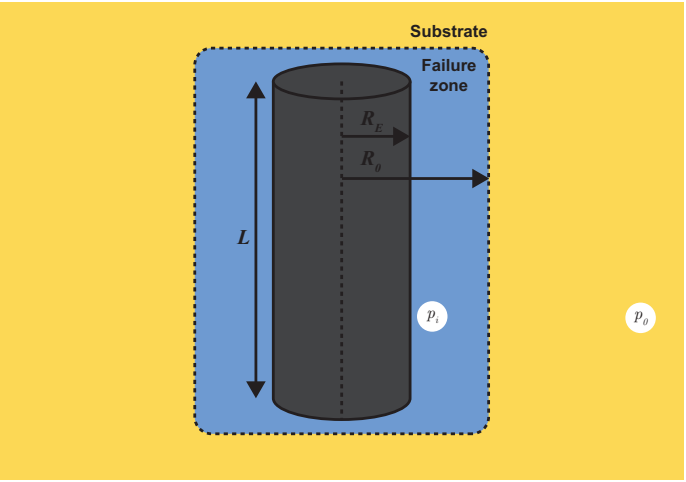

Figure 6: COLLAPSING SOIL MODELED AS A THICK-WALLED PRESSURE VESSEL**.** The RoboClam mechanism is shown in dark gray as having just contracted, with the void around it marked in blue as the failure zone. The soil is around the failure zone in yellow. Labels: R_0 is the radius of the expanded mechanism, R_E is the radius of the contracted mechanism, L is the length of the mechanism, p_i is the pressure in the failure zone, and p_0 is the lateral pressure of the undisturbed soil at infinity.

Combining Eqns. (1) and (2) with the definitions of vertical and horizontal effective stress, as well as the definitions of soil properties K_0 and K_a, results in expressions for the failure radii R_{frv} and $R_{fr\theta}$ [6].

$$\frac{R_{frv}}{R_0} = \sqrt{\frac{p_i - p_0}{\left(\frac{K_a}{K_0} - 1\right)(p_0 - u)}} \tag{3}$$

$$\frac{R_{fr\theta}}{R_0} = \sqrt{\frac{(K_a + 1)(p_i - p_0)}{(K_a - 1)(p_0 - u)}} \tag{4}$$

The failure radii, R_{frv} and $R_{fr\theta}$, are the radial distances at which failure occurs for landslide and annular collapse, respectively. In other words, these are the outer radii of the thick-walled pressure vessel, or the distances after which the soil is no longer affected by the mechanism's collapse. K_a and K_0 are the coefficient of active failure and the coefficient of lateral earth pressure of the soil, respectively, which are both measured soil properties. The pore pressure, u, is caused by the fluid between the soil particles in the general case. However, since we are working with dry soil, $u = 0$, and since our model assumes that the mechanism has just contracted, $p_i = 0$. With these two assumptions, Eqns. (3) and (4) simplify to:

$$\frac{R_{frv}}{R_0} = \sqrt{\frac{1}{\left(1 - \frac{K_a}{K_0}\right)}} \tag{5}$$

$$\frac{R_{fr\theta}}{R_0} = \sqrt{\frac{K_a + 1}{1 - K_a}}. \tag{6}$$

DOMINANT FAILURE MECHANISM

For any soil for which we know K_0 and K_a, we can find the characteristic radius within which the soil collapses for both the landslide and annular collapse cases. In general, these characteristic radii will be different, meaning that landslide and annular collapse will occur within different volumes of soil. If the landslide radius is bigger, then annular collapse will occur within the volume of soil undergoing landslide collapse, and vice versa. Therefore, the larger radius will correspond to the radius of total affected soil. We will call this larger radius the radius of the dominant failure mechanism. We can divide Eqn. (5) by Eqn. (6) to get the ratio of the landslide radius to the annular radius

$$\frac{R_{frv}}{R_{fr\theta}} = \sqrt{\frac{K_a - 1}{\left(\frac{K_a}{K_0} - 1\right)(K_a + 1)}}. \tag{7}$$

If this ratio is greater than one, then landslide collapse dominates. If it is less than one, then annular collapse dominates. Figure 7 shows a plot of the ratio for a range of K_0 and K_a values. Generally, for values of K_0 under about 0.6, landslide collapse dominates, whereas for values of K_0 above 0.6, annular collapse dominates.

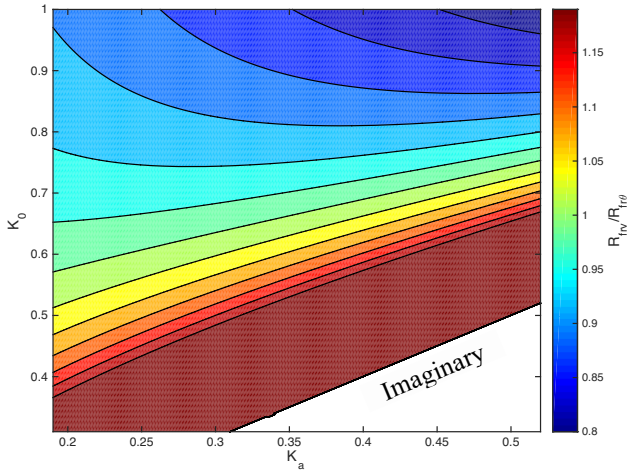

Figure 7: DOMINANT FAILURE MECHANISM GRAPH. Values greater than 1 (red to green) indicate landslide collapse dominance, whereas values less than 1 (green to blue) indicate annular collapse dominance. The bottom corner indicates an imaginary section, where combinations of K_0 and K_a values are not physically possible.

This analysis raises the question of whether there is a correlation between K_0 and K_a values that would allow us to focus on certain areas of Fig. 7. K_a is defined by the geometry of Mohr's circle at failure, and can be expressed in terms of the friction angle [8]:

$$K_a = \frac{1 - \sin(\varphi)}{1 + \sin(\varphi)}. \tag{8}$$

Additionally, there are two correlations for K_0 that have been experimentally determined and are generally accepted by the geotechnical community: one for normally consolidated soils (which have never experienced stresses larger than the ones they are currently experiencing) and one for overconsolidated soils (which have been loaded and then unloaded, for example the soil beneath glaciers that have since melted). The normally consolidated correlation [9] is expressed as

$$K_{0(NC)} = 1 - \sin(\varphi), \tag{9}$$

where $K_{0(NC)}$ is the normally consolidated coefficient of lateral pressure. The correlation for overconsolidated soil [10] is expressed as

$$K_{0(OC)} = \mathrm{K_{0(NC)}} * \mathrm{OCR}^{\sin\varphi}, \tag{10}$$

where $K_{0(OC)}$ is the overconsolidated coefficient of lateral pressure, and *OCR* is the overconsolidation ratio, or the ratio of the maximum past stress experienced to the present stress experienced.

Since Eqns. (8), (9), and (10) are all in terms of the friction angle φ, we can combine them to find correlations between K_0 and K_a and overlay them on the plot in Fig. 7. Figure 8 shows the dominant failure mechanism graph with K_0–K_a correlations for normally consolidated soil (NC) and for overconsolidation ratios (OCR) of two, three, four, and five.

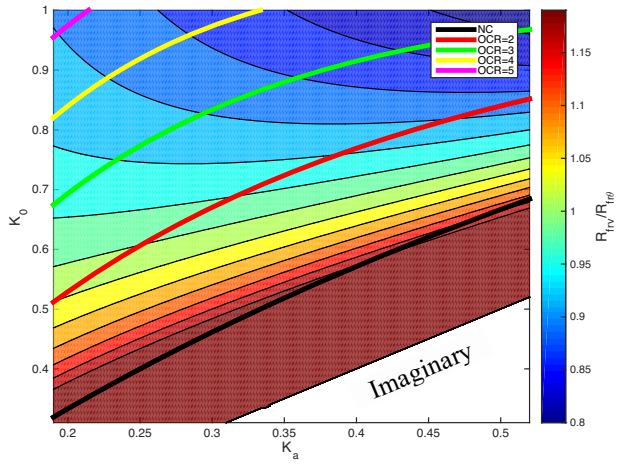

Figure 8: DOMINANT FAILURE MECHANISM GRAPH WITH K_0–K_a CORRELATIONS. Correlations are marked for normally consolidated soil as well as for soil with overconsolidation ratios of two, three, four, and five.

Figure 8 shows that in general, landslide collapse is dominant for normally consolidated soils, whereas annular collapse is dominant for overconsolidated soils. Since both modes of collapse are potentially relevant, we must determine how quickly collapse occurs in each case (and thus discover how quickly the end effector must contract to achieve a zero-stress state).

LANDSLIDE COLLAPSE ANALYSIS

Figure 9 shows a free body diagram of the block of soil that slides diagonally in landslide collapse.

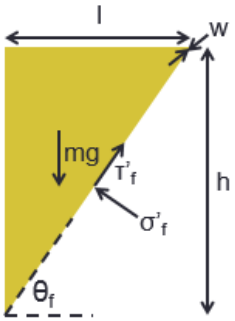

Figure 9: FREE BODY DIAGRAM OF A BLOCK OF SOIL ABOUT TO UNDERGO LANDSLIDE COLLAPSE. Labels: θ_f is the failure surface angle, m is the mass of the block of soil, g is the gravitational constant, τ'_f and σ'_f are the effective shear stress at failure and the effective vertical stress at failure, respectively, and l, w, and h are the arbitrary dimensions of the block of soil.

To determine the time it will take the soil block to move a horizontal distance of δ (the device contraction distance), the

shear and normal stresses on the diagonal plane can be reduced to a horizontal stress of σ'_{hf}. This stress can be expressed as

$$\sigma'_{hf} = \mathrm{K_a} g h (1 - \Phi)(\rho_p - \rho_f), \qquad (11)$$

where g is the gravitational constant, Φ is the void fraction of the soil, or the fraction of the soil volume that is made up of air or fluid rather than of soil particles, ρ_p is the density of the soil particles, and ρ_f is the density of the fluid in the general case [11]. This horizontal stress acts on a projected area of $h*w$, resulting in a horizontal force of

$$\mathrm{F_H} = \mathrm{K_a} g h (1 - \Phi)(\rho_p - \rho_f) h w\,. \qquad (12)$$

Furthermore, the mass of the block is defined as

$$\mathrm{m} = \frac{1}{2} l h w \left[\rho_p (1 - \Phi) + \rho_f \Phi\right]. \qquad (13)$$

Using basic kinematics and assuming an initial velocity of zero for the block of soil, the time to move a distance δ is

$$\mathrm{t} = \sqrt{\frac{2\delta}{\mathrm{a}}} = \sqrt{\frac{2\delta m}{F_H}} = \sqrt{\frac{\delta(\rho_p(1-\Phi) + \rho_f \Phi)}{K_a g (1-\Phi)(\rho_p - \rho_f) tan\theta_f}}\,. \qquad (14)$$

For dry soil, we can assume that ρ_f =0, which simplifies Eqn. (14) to

$$\mathrm{t} = \sqrt{\frac{\delta}{\mathrm{K_a} g tan\theta_f}}\,. \qquad (15)$$

The failure surface angle can be derived from Mohr's circle and is defined as

$$\theta_\mathrm{f} = \frac{\pi}{4} + \frac{\phi}{2}\,. \qquad (16)$$

Using Eqns. (15), (8), and (16), as well as δ = 0.0048m (the contraction distance for the existing RoboClam end effector), we can find the range of possible values for landslide collapse time in typical soils. Soils can typically have a friction angle φ ranging from 17˚ (very weak soils) to 45˚ (very strong soils) [12]. This friction angle range corresponds to a landslide collapse time range of 0.0198s to 0.0266s for the current RoboClam end effector dimensions. RoboClam runs on a pneumatic control system that can contract on the order of 0.03s, so these timescales are a little faster than the norm, but are feasible. They could potentially be reached by increasing the air pressure currently used to control the machine, or by replacing the pneumatic system altogether with a faster linear actuator.

ANNULAR COLLAPSE ANALYSIS

Figure 10A shows the top view of a block of soil about to undergo annular collapse. Similar to the landslide case, there is an effective horizontal stress acting on one side and zero horizontal stress acting on the other. Additionally, there is a frictional force acting on the top and bottom of the soil block as it slides into the void (Fig. 10B). Figure 10C shows a differential angular element of soil about to undergo annular collapse, with the shear and normal forces labeled.

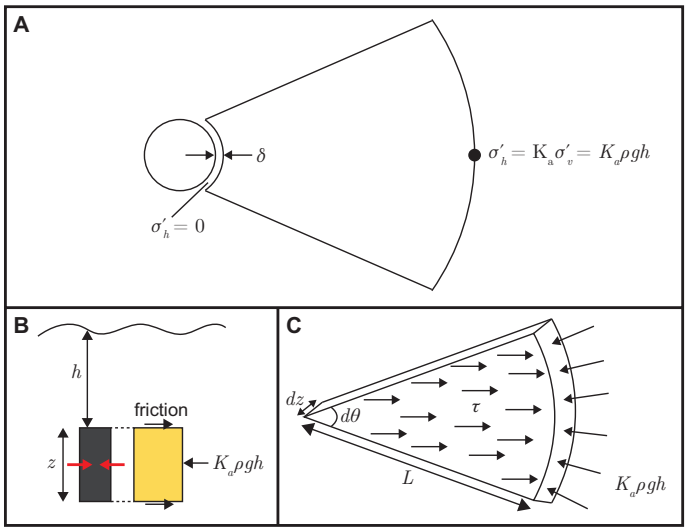

Figure 10: VISUALIZATIONS OF ANNULAR COLLAPSE. A) Top view of a block of soil about to undergo annular collapse. The mechanism has just contracted a distance of δ, leaving a void with an effective stress of zero. At the edge of the affected soil, the horizontal effective stress is defined as K_a multiplied by the vertical effective stress. B) Side view of the mechanism after contraction. The block of soil that will undergo annular collapse is marked in yellow. There is a frictional force caused by the stationary soil above and below the block that opposes the motion. C) Free body diagram of a differential angular element of soil before annular collapse, with the unknown shear force τ labeled. L is the characteristic length of soil collapse, or the distance from the mechanism to the edge of the affected soil mass.

We use a Mohr's circle analysis with a radial-vertical reference frame to quantify the shear stress that corresponds to this state of annular collapse. We know the radial and vertical effective stresses at collapse, defined as

$$\sigma_{\mathrm{vf}}' = \rho g h \qquad (17)$$

$$\sigma'_{\mathrm{rf}} = \mathrm{K_a} \rho g h\,. \qquad (18)$$

Since the soil is at failure, the Mohr's circle will be tangent to the failure envelope. The Mohr's circle must be centered about the midpoint between σ_{vf}' and σ_{rf}', such that they will both correspond to the same shear stress value. These three

qualifications define the Mohr's circle that gives the shear stress encountered in annular collapse (Fig. 11).

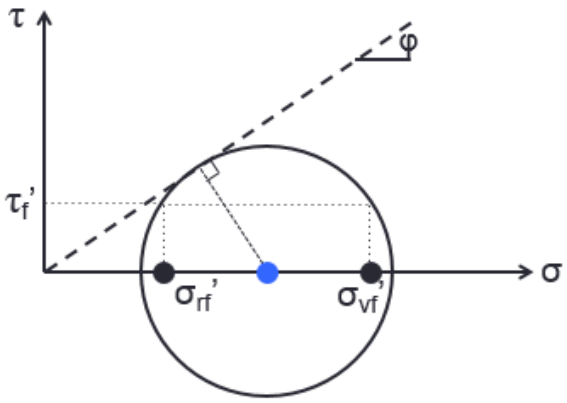

Figure 11: MOHR'S CIRCLE ANALYSIS USED TO DETERMINE THE SHEAR STRESS ENCOUNTERED IN ANNULAR COLLAPSE. The known radial and vertical effective stresses at collapse are plotted, and the midpoint between them is defined as the center of the circle. The Mohr's circle is then defined as the circle tangent to the failure envelope, centered at that point. The frictional shear stress is the stress that corresponds to both the radial and vertical effective stresses on this circle.

Geometrical analysis of Figure 11, coupled with Eqns. (17) and (18), yield the following value for τ_f':

$$\tau = \rho g h \sqrt{K_a - \frac{1}{4}\cos^2\phi\,(1+K_a)^2} \qquad (19)$$

Using Eqn. (19) as the shear force in the free body diagram in Figure 10C and plugging in z as the length of the contracting mechanism yields the following sum of forces:

$$\Sigma F_H = K_a \rho g h z L d\theta - 2\left(\frac{1}{2}L^2 d\theta\right)\left(\rho g h \sqrt{K_a - \frac{1}{4}\cos^2\phi\,(1+K_a)^2}\,\right) \qquad (20)$$

Again using basic kinematics and assuming an initial velocity of zero for the block of soil results in:

$$t = \sqrt{\frac{2\delta}{a}} = \sqrt{\frac{z\delta L}{ghK_a z - Lgh\sqrt{K_a - \frac{1}{4}\cos^2\phi\,(1+K_a)^2}}} \qquad (21)$$

The expression for collapse time depends on L, the characteristic length of the annular collapse. This length is equivalent to $R_{fr\theta}$, which was defined in Eqn. (6) as a function of expanded end effector radius. Plotting Eqn. (6) for the same values of K_0 and K_a that were used in Figs. 7 and 8, as well as overlaying the normally consolidated and overconsolidated soil curves, results in Fig. 12.

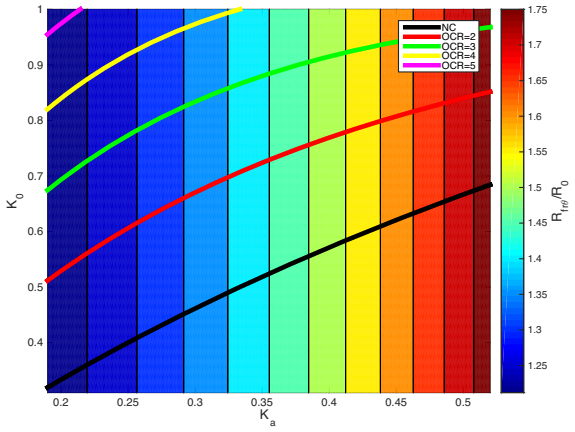

Figure 12: RADIUS OF ANNULAR COLLAPSE GRAPH. K_0—K_a correlations are overlaid for normally consolidated and overconsolidated soil.

Figure 12 shows that $R_{fr\theta}$ is always between R_0 and $2R_0$. As a result, substituting L=R_0 and L=$2R_0$ into Equation (21) yields a range of possible annular collapse times. Using K_a=0.33 (a typical value for soil) and h=0.5m, these values result in an annular collapse time range of 0.0044s to 0.0080s, which are an order of magnitude smaller than the times found for landslide collapse. Additionally, the times scale with $h^{-0.5}$, so if the depth is increased from one-half to one meter, the time range decreases to 0.0032s to 0.0056s. All of these times are not achievable with the current RoboClam setup, and may be difficult to achieve with similar devices.

CONCLUSIONS

For a RoboClam-like device to achieve a zero-stress state in dry soil in a landslide collapse-dominated environment, it must contract in ~ 0.02 seconds. Alternatively, in an annular collapse-dominated environment, it must contract in ~ 0.004 seconds, an order of magnitude more quickly than in the landslide case. Though 0.02 seconds is within the realm of possible contraction times for a mechanism similar to RoboClam, 0.004 seconds is too fast. Therefore, *Ensis*-inspired motions are a feasible digging strategy for landslide-dominated soils, but not for annular-dominated soils. Based on Fig. 8, in general, normally consolidated soils and overconsolidated soils with very small *OCR*s are landslide-dominated. Thus, underground sensor placement by a device similar to RoboClam in dry soil is feasible, but only for soils that have not experienced pressures much larger than the pressures they experience at the time of digging. Further work is needed to experimentally verify these results, but theoretically, it seems plausible for RoboClam burrowing technology to be adapted to dry soil applications.

ACKNOWLEDGMENTS

This work was sponsored by Bluefin Robotics Corporation, Compagnie Générale de Géophysique (CGG), and the MIT Department of Mechanical Engineering.

REFERENCES

[1] Winter V, A., Deits, R., Dorsch, D., 2013. "Critical Timescales for Burrowing in Undersea Substrates Via Localized Fluidization, Demonstrated by RoboClam: A Robot Inspired by Atlantic Razor Clams". In Proceedings of the IDETC/CIE Conference, no DETC2013-12798.

[2] Kundu, P., and Cohen, I., 2004. *Fluid Mechanics*. Elsevier Academic Press.

[3] Richardson, J., and Zaki, W., 1954. "Sedimentation and fluidization: PartI". *Chemical Engineering Research and Design*, 32(a), pp. 35-53.

[4] Lambe, T., and Whitman, R., 1969. *Soil Mechanics*. Wiley & Sons, Inc., New York, pp. 99-100.

[5] Winter V, A., Deits, R., Dorsch, D., Hosoi, A., and Slocum, A., 2010. "Multi-Substrate Burrowing Performance and Constitutive Modeling of RoboClam: A Biomimetic Robot Based on Razor Clams". In Proceedings of the IDETC/CIE Conference, no DETC2010-29060.

[6] Winter V, A., Deits, R., Dorsch, D., Slocum, A., and Hosoi, A., 2014. "Razor clam to RoboClam: burrowing drag reduction mechanisms and their robotic adaptation". *Bioinspiration and Biomimetics*, 9(3), April, pp. 4-5.

[7] Timoshenko, S., and Goodier, J., 1970. *Theory of Elasticity*, 3rd ed. McGraw-Hill, New York, pp. 68-71.

[8] Lambe, T., and Whitman, R., 1969. *Soil Mechanics*. Wiley & Sons, Inc., New York, pp. 164.

[9] Jaky, J., 1944. "A nyugalmi nyomâs tényezöje (The coefficient of earth pressure at rest)". *Magyar Mérnok és Epitész Egylet Közlönye (Journal for Society of Hungarian Architects and Engineers)*, October, pp. 355-358.

[10] Mayne, P. and Kulhawy, F., 1982. "Ko-OCR Relationships in Soil". *Journal of the Geotechnical Engineering Division,* ASCE, 108(6), pp. 851-872.

[11] Winter V, A., 2011. "Biologically Inspired Mechanisms for Burrowing in Undersea Substrates". PhD Thesis, Massachusetts Institute of Technology, Cambridge, MA, May.

[12] Peck, R., Hanson, W., and Thornburn, T., 1974. *Foundation Engineering*. Wiley & Sons, Inc., New York.